Concrete-Filled Structural Hollow Sections in Fire: Accounting for Heat Transfer across a Gap

PAPER REF: 2677

HEAT TRANSFER ACROSS A GAP – WITH RELEVANCE TO ANALYSIS OF CONCRETE-FILLED STEEL TUBES IN FIRE

Eoin O'Loughlin[1(*)], David Rush[2], Luke Bisby[3]
[1]AECOM, St Albans, UK
[2, 3]BRE Centre for Fire Safety Engineering, University of Edinburgh, Edinburgh, UK
(*) *Email:* eoin.oloughlin@aecom.com

ABSTRACT

Concrete-filled steel hollow structural (CFS) sections are an increasingly popular means of supporting large compressive loads in structures (i.e. in columns). Efficient in their load carrying capacity, they are architecturally appealing and offer numerous advantages in design and construction. Whilst the design of CFS sections at ambient temperatures is reasonably well understood, and models to predict the strength and failure modes of these elements at ambient temperatures correlate well with observations from tests, this appears not to be true in the case of fire resistant design. The limited understanding is owed to number of knowledge gaps that continue to surround their thermal response and structural behaviour in fire. This paper focuses on a potentially important knowledge gap: the significance on heat transfer of the air gap that typically forms at the interface between the steel tube and concrete core when a CFS section is exposed to fire. The purpose of the research is to investigate the impact that the width of the air gap may have on the heat transfer within the section. To achieve this, a one-dimensional finite difference model of the heat transfer through a CFS section was developed and validated against the results of an experimental programme consisting of approximately 1-D thermal loading of specimens consisting of a steel plate and concrete mass, separated by air gaps of various known widths. The model is shown to reasonably predict the temperature evolution in the concrete mass and is thus deemed to account for the heat transfer physics occurring in the air gap and the resulting insulating effects on the concrete core. The model is subsequently used to propose a correlation between air gap width and rate of heat transfer between steel and concrete. The rate of heat transfer is shown to be considerably reduced for larger air gap widths, highlighting the importance of including air gap formation and development during heat transfer analyses of CFS sections.

INTRODUCTION

Concrete-filled steel hollow structural (CFS) sections are an economical and aesthetically appealing means of supporting large compressive loads and they are increasingly popular in design and construction (Rush et al., 2010). Consisting of hollow steel tubular sections which are filled with concrete, CFS columns have superior load carrying capacity and structural resistance to fire when compared with unfilled hollow steel sections or reinforced concrete columns. Structurally, the two components of a CFS column work together, in that the steel casing offers lateral restraint to the concrete core, allowing it to attain its maximum compressive strength, while the concrete improves the resistance to elastic local buckling of the steel (Kodur, 2007). There are many other advantages associated with CFS columns, including reduced cross-sectional area when compared with conventional concrete columns, corrosion protection provided to the concrete by the steel tube, and considerable appeal to architects owing to their attractive surface finish. CFS sections also allow for rapid construction, since phased assembly can be implemented with the pre-fabricated steel tubes

acting as permanent, weather-proof formwork for the concrete pouring operations that follow; thus reducing forming and stripping costs (Leon and Griffis, 2005). The benefit of CFS columns which is of most relevance to the current study is that the combination of steel tube and concrete core serves to enhance the load carrying capacity of the column during fire. The concrete can act as a thermal sink as well as accommodating a portion of the steel's axial loading when the column is heated during a fire (Leon and Griffis, 2005). This improved structural performance in fire means that, in some cases, the required fire resistance time for a CFS column can be achieved without the need for supplemental fire protection (Kodur, 2005). CFS columns thus provide economical structural fire design solutions while imposing minimal impact on the aesthetics and usable space within a building.

For the fire resistance design of most common types and sizes of CFS columns, official prescriptive guidance documents (CEN, 2005; CEN, 2008) are available, as well as several guidance publications produced by researchers (Kodur, 2007; Lennon et al., 2007; Wang and Orton, 2008; Aribert et al., 2008; Park et al., 2008). Much of the available guidance was developed for conventional applications based on large-scale standard furnace tests and computer modelling of short, concentrically loaded, small-diameter columns envisioned for use in braced frames using normal strength concrete (Rush et al., 2010). Increasingly however, high-performance CFS columns incorporating high-strength concrete and/or very large cross-sections are being specified in the design and construction of large multi-storey structures. The structural performance of modern CFS columns in realistic fire and loading conditions is not well established and their design often falls outside the scope of the available guidance. Current design approaches are limited in scope, and this makes structural fire design of CFS columns using performance-based approaches difficult to defend to approving authorities.

During heating of a CFS column, many thermal and structural response phenomena occur that affect structural failure but which cannot currently be predicted with confidence (Wang and Orton, 2008). Several knowledge gaps exist that are currently limiting the formulation of comprehensive guidance for the fire resistance design of such columns. One area of uncertainty is the effects of the development of air gaps which form at the steel-concrete interface when CFS columns are exposed to fire. During heating, the variation in thermal expansion between the steel tube and concrete core can cause separation of the steel tube from the concrete and the development and growth of an air gap. While ignoring the development of an air gap in analysis of CFS sections is generally thought to be conservative for unprotected CFS columns (Rush et al., 2010), accounting for the presence of the gap considerably improves the accuracy of prediction of temperature distribution within a CFS column during fire; this has been demonstrated by Ding & Wang (2008) and Renaud (2004) where the presence of an air gap was explicitly incorporated into computational analyses – albeit by adopting a gap of constant thickness with an assumed associated thermal resistance imposed (so as to match test data.) The influence of an air gap on the thermal response, and thus the structural performance, of CFS sections remains poorly understood and has yet to be quantified.

To date, the majority of researchers have chosen not to consider the formation of an air gap in their analyses, instead assuming perfect thermal contact between the concrete core and steel tube. In reality, the formation, development, and heat transfer physics which are at play are highly complex; they vary with time and depend on a range of factors such as the type of concrete being used, the thickness of steel tube, the interface mechanical properties, and the rate of heating. The current study investigates, in a controlled manner, the impact that the air

gap might have on the thermal response of CFS columns exposed to fire conditions. A one-dimensional heat transfer model has been developed and is validated against tests involving a series of idealised 1-D experiments. This allows advancement of the simplified means employed in previous research and realistic accounting for the heat transfer physics in the air gap. The numerical predictions and can then be used to examine the impact of an evolving air gap on the heat transfer through a real section. The insights gained help to better understand and define the thermal response of CFS columns in fire, aid the development of robust heat transfer models for these sections, and contribute to the advancement of performance based structural fire design procedures.

EXPERIMENTAL PROGRAMME

The experimental programme was intended to investigate the heat transfer and cross-sectional temperature profile evolution in a vertical segment of a CFS section exposed to fire. The specimens tested were based on an assumed infinitely large CFS section, where the steel plate facing the fire can be considered to be flat, thus allowing a simplified 1-D heat transfer experiment. During the heating of a real CFS column, differential thermal expansion occurs between the steel and concrete of the composite column due to their different rates of heating, thermal gradients arising in the section, and the materials' respective coefficients of thermal expansion. This differential thermal expansion promotes the formation of the air gap, the size of which is dependent on several factors. The experiments were designed not to assess the external factors that influence the *evolution* of the air gap, but to look specifically at the air gap's influence on the thermal response of the section. This was achieved by explicitly separating the steel and concrete elements of the specimens by a constant distance (set at 0mm, 1mm, 3mm, or 5mm) and then recording the temperature evolution at specific points within the specimen when heated using a radiant panel with a well characterised incident heat flux. The experimental program thus allowed observation of the influence of the air gap on the heat transfer through the section and provided data for model validation.

Specimen Preparation

The specimens are shown schematically in Fig. 1 and were 300 x 300 x 125 mm concrete blocks faced with 250 x 250 x 8 mm steel plates. The steel plates were made from mild structural steel and the concrete was a high strength, self-compacting hybrid steel and polypropylene fibre (45 kg/m^3 and 2 kg/m^3 respectively) reinforced concrete mix. The mix design was chosen based on a companion project which is interested in supporting the use of fibre reinforced concrete infill materials as replacement for traditional reinforcing steel cages. The concrete had a moisture content of between 5.0 and 5.8 % by mass and a compressive cylinder strength of 58MPa at the time of testing. The concrete was cast directly onto the steel plates so as to precisely match any imperfections on the steel plates so that when the air gap was artificially created (using a series of steel spacers around the perimeter of the steel plate) a consistent air gap was assured. The perimeter of the air gap was sealed using high temperature ceramic sealant to prevent convective heat loss from the gap and ensure that the heat transfer across the gap was as realistic as possible (Fig. 1). The dimensions and materials used for the specimens are representative of realistic CFS columns and allowed the influence of the air gap to be studied in a controlled manner. Eight Type K thermocouples were used in each test and were placed as shown in Fig. 1; all data were acquired at 10 Hz.

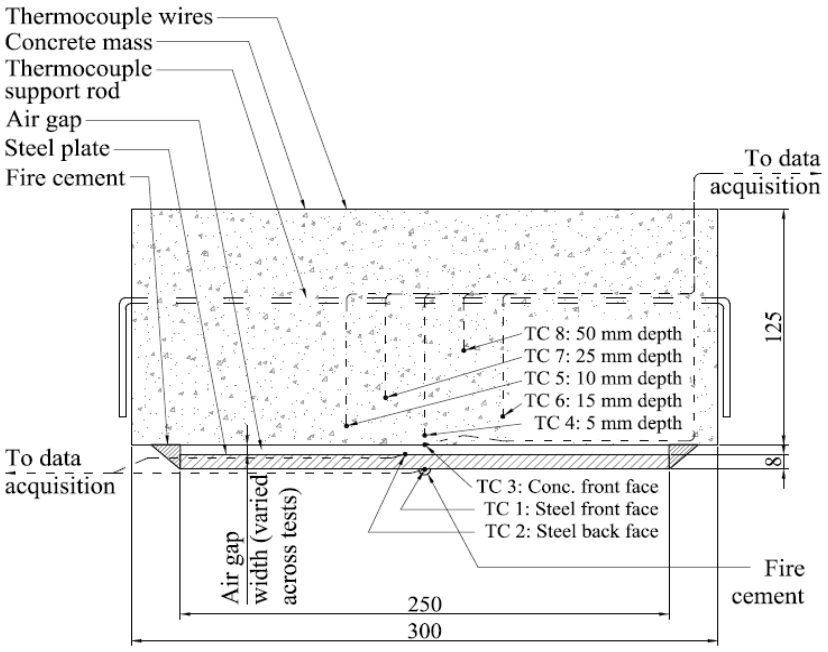

Fig. 1. Test specimen details

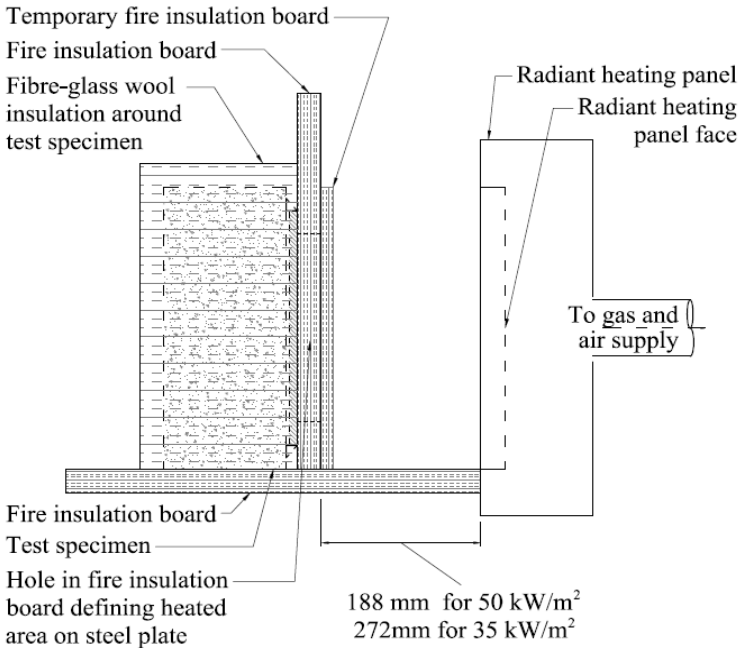

Fig. 2. Test setup

Test setup

The test setup, shown in Fig. 2, had the test specimen vertically positioned behind a ceramic insulation board containing a 200 x 200 mm opening through which heating was applied centrally on the steel plate. A layer of fibre-glass wool was wrapped around the top and sides of the specimen to prevent lateral thermal losses, thus promoting a 1-D heat transfer regime. At the outset of the experimental programme, the average heat flux produced by the radiant

heating panel over the centralised 200 x 200 mm exposed area was measured at various distances from the front face of the radiant panel which was used to heat the samples (Fig. 2). The heat fluxes given in Fig. 2, and the corresponding separation distances between the radiant heating panel and the front face of the steel plate, were selected to represent values for heating effects roughly equivalent to the ISO 834 Standard Fire (Babrauskas, 1995). It should be noted that the heat fluxes varied by ±10% over the heated area.

Testing Procedure

Prior to subjecting the specimens to thermal loading, the radiant heating panel was ignited and allowed to stabilize at a constant heat flux while a temporary fire-insulation board was positioned to shield the 200 x 200 mm opening through which the specimens were heated (Fig. 2). The rate of combustible gas flow supplied to the radiant heating panel was maintained at a pre-defined value by an automatic flow control meter. Once the front face of the steel plate reached 35° C (due to heat transfer through and around the fire-insulation board) as recorded by TC 1 (Fig. 2), the temporary fire-insulation board was removed and rapid heating of the specimens commenced. The heating continued for 60 minutes, after which the combustible gas supply to the radiant panel was turned off and the fire-board was repositioned in front of the steel plate, allowing the specimen to cool slowly for a further 60 minutes during which time temperature measurements were recorded.

Testing Programme

The experimental program, shown in Table 1, was divided into two phases; Phase 1 consisted of eight tests in which the air gap was varied from 0 to 5 mm (with repeat tests at each air gap width); this was immediately followed by Phase 2, consisting of seven tests in which additional repeat tests were performed and the incident heat flux was investigated. A breakdown of the individual experiments that were conducted and a summary of the specifics of each test are given in Table 1. During Phase 1, two tests were carried out using each of the following imposed air gap widths: 0, 1, 3 and 5 mm; these were chosen to cover the range of gap widths assumed to be present in experimental full scale tests based on a review of the available literature (Kodur, 2007; Ding and Wang, 2008; Rush et al., 2010). After the initial eight tests had been carried out and their results had been observed and assessed, the particulars of Phase 2 were established. The purpose of Phase 2 was to allow for additional test variations of possible interest to be explored and for repeat tests if necessary. Due to a mechanical failure in the test apparatus' gas supply, the number of tests remaining used explore different variables was diminished, so a reduction in the level of initial imposed heat flux was used, from the intended 50 kW/m^2 in Phase 1 to 35 kW/m^2 in Phase 2. As shown in Table 1, test repeats were carried out for a heat flux of 50 kW/m^2 using air gaps of 0 mm and 1 mm. The 35 kW/m^2 heat flux test with 1 mm air gap was also repeated, in this case as a result of the heating panel gas supply running out during testing. The data obtained from Tests 3, 4 and 13 all suffered some kind of testing failure and are thus not considered in any of the analysis or discussion.

RESULTS AND DISCUSSION

Figures 3 and 4 show typical samples of temperature data acquired during testing for each of the thermocouples. These plots allow initial qualitative assessment of the heat transfer across the air gap. Comparing the results of the different tests, it can be seen that as the air gap width increases, the steel temperatures increase and concrete temperatures decrease. This is expected and is due to the air gap acting as an insulator.

Table 1. Details of the experimental programme

Test	Heat Flux	Air Gap	Concrete Batch	Comments	Temperatures after 60 minutes of heating (° C)							
					Steel		Concrete					
	(kW/m^2)	(mm)			TC1 Front face	TC2 Back face	TC3 Front face	TC4 5 mm depth	TC5 10 mm depth	TC6 15 mm depth	TC7 25 mm depth	TC8 50 mm depth
Phase 1												
1	50	0	1	--	550	518	445	372	314	275	219	144
2	50	0	1	--	561	515	424	345	294	286	209	147
3	50	1	1	Fan malfunction at ~ 40 min	531	494	380	322	248	243	204	139
4	50	1	1	Fan malfunction at ~ 30 min	185	192	184	180	167	164	156	126
5	50	3	1	TC 5 malfunction throughout	590	564	407	318	*(340)*	247	196	128
6	50	3	2	TC 3 malfunction until ~ 25 min	590	549	405	308	270	239	191	129
7	50	5	2	Data logger malfunction at 60 min	589	566	405	341	283	244	201	133
8	50	5	2	--	590	568	400	332	266	261	206	129
Phase 2												
9	50	0	2	--	572	547	485	400	351	270	255	140
10	50	1	2	--	578	553	433	358	299	263	208	133
11	50	1	3	--	585	569	460	391	332	254	234	132
12	35	0	3	--	433	385	313	268	218	203	164	120
13	35	1	3	Gas supply ran out at ~ 25 min	385	373	262	214	203	172	152	109
14	35	5	3	--	462	428	251	222	175	157	134	106
15	35	1	3	TC 7 malfunction throughout	423	398	251	209	196	158	*(113)*	82

The response of the steel plates is characterised by two ‘phases’. The first phase is characterised by an immediate, steep increase in temperature. The temperature continues to rise at a relatively rapid rate for 10-15 minutes after the start of the heating. The second phase is characterised by a relatively constant reduced rate of temperature increase in the steel from about 15 minutes to the end of the tests.

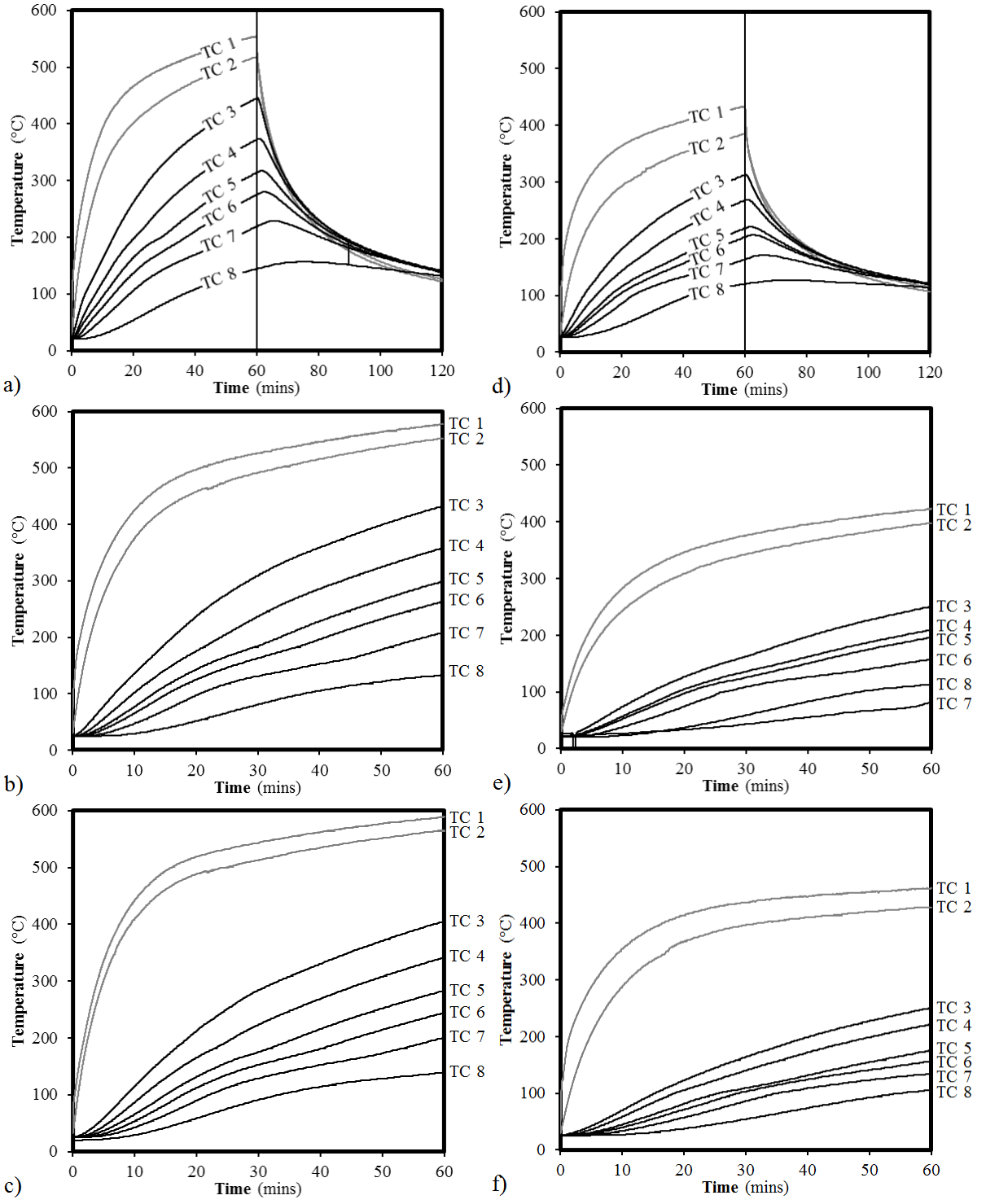

Fig. 3.Examples of temperature profiles in specimens with a) 0 mm; b) 1 mm; and c) 5 mm air gaps, exposed to a 50 kW/m^2 heat flux, and in specimens with d) 0 mm; e) 1 mm; and f) 5 mm air gaps, exposed to a 35 kW/m^2 heat flux.

The temperatures experienced by the concrete were significantly lower than those in the steel, with a more gradual and less variable rate of temperature increase. The difference in the rate of heating between the two components is highlighted by the fact that the greatest temperature difference between the back face of the steel and the front face of the concrete was observed

early in the heating, at approximately 10-15 minutes. This is also seen during the cooling phase (Figs. 3(a) and 3(d)), where after the thermal load was removed, the steel temperatures dropped off relatively rapidly whereas temperatures continued to increase for a short period in the concrete before beginning to decrease. The peak temperatures in the concrete 50mm from the concrete surface were observed 15-20 minutes after the heating was removed.

As expected, the air gap is shown to act as an insulator, and the influence that the size of air gap had on the thermal behaviour of the specimens is considerable. The general trend is that a larger air gap results in higher steel temperatures and lower concrete temperatures. The test results indicate that as the air gap width increases the heat transfer between the steel and the concrete decreases, however the trend is not linear. Figure 4 shows a comparison of the temperatures on the back face of the steel plate and the front face of the concrete block with differing air gap widths. The temperature difference between the two faces increases considerably when a 1 mm air gap is introduced. However, as the air gap increases to 3 mm in width, and further to 5 mm, the degree to which the temperature difference increases is reduced.

The tests have clearly shown that an air gap has a substantial influence on heat transfer within CFS sections. The omission of the air gap during design could lead (in terms of a thermo-mechanical analysis) to (a) an under-prediction of steel temperatures, resulting in an over-prediction of the time to failure for CFS sections in which the structural fire performance of the steel tube is more critical; or (b) an over-prediction of concrete temperatures resulting in inefficient design of CFS sections where the performance of the concrete core is more critical.

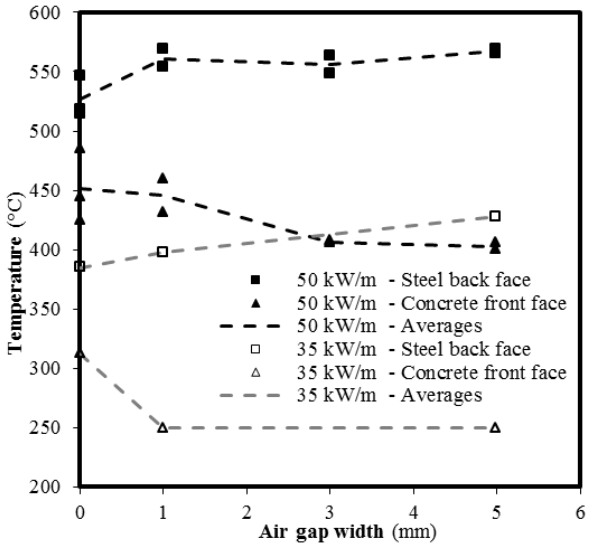

Fig. 4: Variation in maximum temperatures with air gap width

MODELLING

A simple 1-D heat transfer model was developed to simulate the heat transfer from a radiant panel into a vertical steel plate, across an air gap, and into and a concrete mass. The model was developed within a spreadsheet using an explicit finite difference formulation based upon an elemental conservation of energy and driven by a heat flux incident upon the front face of the steel. Using fundamental heat transfer physics, a series of analytical equations were

established upon which the finite difference heat transfer algorithm operated. The heat transfer equations formulated are similar to those used in previous research on modelling the structural fire behaviour of CFS sections (e.g. Lie and Kodur, 1996; Lie and Irwin, 1996). From these finite difference formulations it was possible to compute the temperature of any element at any time step and thus predict the temperature evolution within the sections.

Applying the principle of conservation of energy to each layer element, the energy stored, ΔQ_{st}, by an element in a particular time period is given by the difference between the energy transferred into the element, Q_{in}, and the energy transferred out of the element, Q_{out}.

$$\Delta Q_{st} = Q_{in} - Q_{out} \quad (1)$$

For each element, Q_{in} and Q_{out} were determined by considering how the conductive, convective and radiative modes of heat transfer applied and then calculating their respective contributions.

Conduction

Using Fourier's law (Eq. 2), the rate of heat transfer through a material is proportional to the negative gradient in the temperature and to the area, at right angles to that gradient, through which the heat is flowing. Fourier's Law is:

$$\dot{q}_n'' = -k_n \frac{\delta T}{\delta n} \quad (2)$$

where $\dot{q}_n''$ is the heat transfer rate in the positive *n* direction per unit area, k_n is the thermal conductivity coefficient of the transfer medium in the direction *n*, and $\delta T/\delta n$ is the temperature gradient in the direction *n*. This law is based on the assumption that the substance through which the transfer is taking place is a solid *or* incompressible and motionless liquid or gas.

Combining this relationship with the second law of thermodynamics, which dictates that $\dot{q}_n''$ must always flow towards regions of lower temperature, the conduction equation for the temperature function *T(x,y,z,t)* within a differential volume in Cartesian coordinates can be expressed by the heat diffusion differential equation (Incropera and Dewitt 2002):

$$\frac{\delta}{\delta x}\left(k\frac{\delta T}{\delta x}\right) + \frac{\delta}{\delta y}\left(k\frac{\delta T}{\delta y}\right) + \frac{\delta}{\delta z}\left(k\frac{\delta T}{\delta z}\right) + \dot{q}'' = \rho C_p \frac{\delta T}{\delta t} \quad (3)$$

where $\dot{q}''$ represents heat generation within the material, ρ and C_p are the density and the specific heat of the material respectively and *t* is time.

If the heat transfer is assumed to occur in one dimension only, as is the case in this model, the heat transfer via conduction in the *x*-direction is given by:

$$\frac{\delta}{\delta x}\left(k\frac{\delta T}{\delta x}\right) + \dot{q}'' = \rho C_p \frac{\delta T}{\delta t} \quad (4)$$

The physical significance of the various terms in Equation 4 demonstrates that it is simply a mathematical description of the principle of conservation of energy. The first term represents heat transfer into or out of the differential volume due to heat conduction, the second term

accounts for heat generation in the differential volume and the term on the right hand side represents the heat stored in the differential volume per unit time.

The above differential equation has been used in this study, with appropriate simplifications, (for example assuming that the temperature of the air in the gap is equal to the average temperature of the back face of the steel and the front face of the concrete, and that there was no mass transfer in terms of water vapour in the analysis), and boundary conditions, to arrive at the equations employed in the numerical model for the heat transfer through the solids, i.e. the steel and concrete. However, in representing the heat transfer across the air gap, the assumption that the transferring medium is a solid or incompressible and motionless liquid or gas is not valid and thus Fourier's Law of heat conduction does not apply. Instead, the effects of convection between the back face of steel and front face of the concrete had to be considered in conjunction with conduction, while the radiative heat transfer between the two surfaces also had to be evaluated.

Convection

Convective heat transfer from a vertical surface may be expressed in terms of Newton's law of cooling, which presents the relationship between the rate of heat transfer per unit area $\dot{q}''$ and the temperature difference between the surface and ambient as (Bejan, 1993):

$$\dot{q}'' = \bar{h}(T_w - T_\infty) \quad (5)$$

where $\bar{h}$ is the average convective heat transfer coefficient integrated over the entire surface and T_w and T_∞ are the vertical wall surface temperature and the ambient temperature, respectively. The heat transfer coefficient $\bar{h}$ depends on the flow configuration, fluid properties, dimensions of the heated surface and also on the temperature difference between the heated surface and the surrounding medium. The association given by Equation 5 is therefore non–linear, with $\bar{h}$ being generally expressed in terms of the Nusselt number, *Nu*, a non-dimensional parameter defined as:

$$\overline{Nu} = \frac{\bar{h}L}{k} \quad (6)$$

where *L* is the height of the vertical surface and is as such a characteristic dimension particular to the surface. The Nusselt number, *Nu*, is determined from a variety of relationships with dimensionless numbers based upon the geometry of the heat transfer system, the temperature gradient across the system, the properties of the fluid, and the flow regime. The non-dimensional quantities are namely the Prandtl number, *Pr* (≈ 0.72 and constant for air), the Rayleigh number, Ra_y (based on local altitude, *y*), and the Grashoff number, *Gr*:

$$Ra_y = \frac{g\beta(T_w - T_\infty)y^3}{\alpha\nu} \quad (7)$$

$$Gr_w = \frac{g\beta\rho^2(T_w - T_\infty)w^3}{\mu^2} \quad (8)$$

in which *g* is acceleration due to gravity, β is the coefficient of thermal expansion of the fluid, α is the thermal diffusivity of the surface, ρ, ν and μ are the density, kinematic viscosity, and

dynamic viscosity of the fluid, respectively, T_w and T_∞ are the temperatures of the surface and of ambient, respectively.

In the context of the heat transfer across the air gap between steel and concrete in a CFS column, the applicable convective regime is that of natural convection within a thin vertical enclosure. De Graff and Van Der Held (1952) showed that the overall heat transfer this scenario can be represented using a single "conductance" term that considers the coupled effects of both conduction and convection. The conductance, h_{gap}, is obtained by substitution for $\bar{h}$ in Equation 6, wherein for vertical air layers such as the one in question the air gap Nusselt number, Nu_{gap}, is given by (De Graff and Van Der Held, 1952) as:

$$Nu_{gap} = \begin{cases} 1 & Gr_w < 7 \times 10^3 \\ 0.0384\ \mathrm{Gr}_w^{0.37} & 10^4 < Gr_w < 8 \times 10^4 \\ 0.0317\ Gr_w^{0.37} & Gr_w > 2 \times 10^5 \end{cases} \quad (9)$$

where Gr_w is the dimensionless Grashof number for the air gap (based on the air gap width, w). For the tests outlined in the current paper, the Grashof number, Gr_w, did not exceed 7 x 10^3 and therefore the Nusselt number, Nu_{gap}, can be assumed as equal to 1.

Convective heat transfer at both the front surface of the steel and back surface of the concrete were greatly simplified in the model. At the back face of the concrete, the temperature difference between the concrete and ambient was deemed to remain sufficiently small throughout testing that the amount of heat loss to the surroundings was negligible and need not be considered. At the front face of the steel, heat transfer via convection from the steel to the environment was accounted for through the use of a single convective heat loss coefficient, h_c. Due to the complex physics involved in such heat transfer problems and the case-specific nature of the heat loss coefficients, h_c was used as a user-defined term that could be altered to manually produce temperature evolution predictions for the steel front face elements that correlated well with the experimental data. While this is not ideal, the focus of the current study is on the heat transfer across the air gap, so that the heat transfer to the steel front face is not of central importance (however important for calculations in practice).

Radiation

To incorporate radiative heat transfer across the air gap in the numerical model, the well-known equation for radiative heat transfer between two infinite parallel plates of area $A_1 = A_2 = A$ was employed:

$$q_{1\to 2} = \sigma \varepsilon A (T_1^4 - T_2^4) \quad (10)$$

where $q_{1\text{-}2}$ is the net radiation between bodies *1* and *2*, σ is the Stefan-Boltzmann constant (= 5.669 x 10^{-8} W/m^{2}K^4), T_1 and T_2denote the temperatures of surfaces *1* and *2*, respectively, and ε is the relative emissivity between the two surfaces, where $\varepsilon = \varepsilon_1\varepsilon_2$. Emissivity values are specific for given surfaces and are dependent on many factors such as smoothness, cleanliness, and colour. For simplicity, uniform values were used in the numerical model, with steel emissivity, ε_s and concrete emissivity, ε_c taken as 0.32 and 0.97 respectively after Bejan (1993).

Finite Difference equations

Manipulating the above heat transfer equations and employing them in the energy balance approach outlined, finite difference formulations have been developed through which the temperature at any time-step in any element can be calculated (Equations 17-22 in Table 2). With an incident heat flux, Q_{in}, of either 50 kW/m^2 or 35 kW/m^2 acting upon the steel front face element as the driving force for the analytical algorithm, the model can be used to create predictions for the temperature profile evolution within representations of the specimens in the experimental program. Standard values for material properties, and expressions for the variation of material properties with temperature, were used in the application of the heat transfer equations (CEN, 2005; CEN, 2008).

Table 2. Details of the numerical modelling approach

Element		**Energy Balance Equations: ΔQ_{st} =**	**Finite Difference Equations: Element temperatures (time increment = Δt)**
Steel			
Front face	s,0	$\Delta Q_{st} - Q_{out}^{conv.} - Q_{out}^{cond.}$ (11)	$T_{s,0}^{i} = T_{s,0}^{i-1} + \frac{\Delta t}{\rho_s C_s \Delta x_s}\left[Q_{in} - h_c\left(T_{s,0}^{i-1} - T_{\infty}\right) - \left(\frac{k_{s,0}^{i-1} + k_{s,1}^{i-1}}{2}\right)\left(\frac{T_{s,0}^{i-1} - T_{s,1}^{i-1}}{\Delta x_s}\right)\right]$ (17)
Internal	s,m	$Q_{in}^{cond.} - Q_{out}^{cond.}$ (12)	$T_{s,m}^{i} = T_{s,m}^{i-1} + \frac{\Delta t}{2\rho_s C_s \Delta x_s^2}\left[\left(k_{s,m-1}^{i-1} + k_{s,m}^{i-1}\right)\left(T_{s,m-1}^{i-1} - T_{s,m}^{i-1}\right) - \left(k_{s,m}^{i-1} + k_{s,m+1}^{i-1}\right)\left(T_{s,m}^{i-1} - T_{s,m+1}^{i-1}\right)\right]$ (18)
Back face	s,n	$Q_{in}^{cond.} - Q_{out}^{cond.} - Q_{out}^{conv.} - Q_{out}^{rad.}$ (13)	$T_{s,n}^{i} = T_{s,n}^{i-1} + \frac{\Delta t}{\rho_s C_s \Delta x_s}\left[\left(\frac{k_{s,n-1}^{i-1} + k_{s,n}^{i-1}}{2}\right)\left(\frac{T_{s,n-1}^{i-1} - T_{s,n}^{i-1}}{\Delta x_s}\right) - h_{gap}\left(T_{s,n}^{i-1} - T_{c,0}^{i-1}\right) - \varepsilon\sigma\left(\left(T_{s,n}^{i-1}\right)^4 - \left(T_{c,0}^{i-1}\right)^4\right)\right]$ (19)
Concrete			
Front face	c,0	$Q_{in}^{cond.} + Q_{in}^{conv.} + Q_{in}^{rad.} - Q_{out}^{cond.}$ (14)	$T_{c,0}^{i} = T_{c,0}^{i-1} + \frac{\Delta t}{\rho_c C_c \Delta x_c}\left[h_{gap}\left(T_{s,n}^{i-1} - T_{c,0}^{i-1}\right) + \varepsilon\sigma\left(\left(T_{s,n}^{i-1}\right)^4 - \left(T_{c,0}^{i-1}\right)^4\right) - \left(\frac{k_{c,0}^{i-1} + k_{c,1}^{i-1}}{2}\right)\left(\frac{T_{c,0}^{i-1} - T_{c,1}^{i-1}}{\Delta x_c}\right)\right]$ (20)
Internal	c,m	$Q_{in}^{cond.} - Q_{out}^{cond.}$ (15)	$T_{c,m}^{i} = T_{c,m}^{i-1} + \frac{\Delta t}{2\rho_c C_c \Delta x_c \Delta x_c^2}\left[\left(k_{c,m-1}^{i-1} + k_{c,m}^{i-1}\right)\left(T_{c,m-1}^{i-1} - T_{c,m}^{i-1}\right) - \left(k_{c,m}^{i-1} + k_{c,m+1}^{i-1}\right)\left(T_{c,m}^{i-1} - T_{c,m+1}^{i-1}\right)\right]$ (21)
Back face	c,n	$Q_{in}^{cond.} - Q_{out}^{conv.}$ (16)	$T_{c,n}^{i} = T_{c,n}^{i-1} + \frac{\Delta t}{\rho_c C_c \Delta x_c \Delta x_c}\left[\left(\frac{k_{c,n-1}^{i-1} + k_{c,n}^{i-1}}{2}\right)\left(\frac{T_{c,n-1}^{i-1} - T_{c,n}^{i-1}}{\Delta x_c}\right) - h_c\left(T_{c,n}^{i-1} - T_{\infty}\right)\right]$ (22)

Validation & Calibration

To justify the applicability of the analytical formulations to the heat transfer scenario in question, it was necessary to validate the numerical solutions. The validation process involved comparing the predictions of the numerical model against the results of the experiments. It was found initially that the heat transfer across the gap was not properly accounted for in the model when the test results were compared to those of the model. To account for this and to improve the accuracy of the predictions an empirical factor, *n*, was introduced to the formulation of h_{gap} as shown in Eq. 23, where the air gap conductance coefficient, h_{gap}, used in Equations 19 and 20 is given by a variation of Equation 6:

$$h_{gap} = n\left(\frac{k}{L}Nu_{gap}\right) \quad (23)$$

It was found also that the size of the parameter, *n*, increased as the size of the air gap increased and was also dependant on the heat flux applied to the steel face and so an *n* – w relationship can be established.

The initial aim of the modelling was to develop a valid numerical heat transfer model that would be driven by an imposed heat flux of user-defined magnitude. This purely analytical model was created by applying the analytical formulations described above and using standard relationships for material property variations with temperature (CEN, 2005; CEN, 2008). In conducting this numerical analysis however, it became apparent that the temperature evolution of the steel plate could not be validly represented using purely analytical means. For the solutions to correlate with the test results, it was necessary to impose an unrealistically large convective heat loss coefficient, h_c, in Equation 17. Reasons for this could include misuse of heat transfer theory in the finite difference formulations, errors in applying the formulations in the numerical model, the use of incorrect material property values (such as emissivity) or an over-prediction of the heat flux applied during testing.

To be able to rely on the input heat to the system it was decided to impose the steel temperatures recorded on the back face of the steel in the experimental programme upon the steel elements in the analytical representation. It was deemed that this approach would allow for accurate and valid numerical solutions to be attained, without compromising the primary objective of examining the impact that the size of the air gap may have on the heat transfer. A hybrid model was thus created to analyse the heat transfer across the gap with the analytical formulation beginning with the heat transfer from the back face of the steel plate to the front face of the concrete mass (Equation 20). The remaining finite difference equations through the concrete mass (Equations 21 and 22) remained the same as for the purely analytical model.

The accuracy of the model's representation of the concrete's thermal response was investigated by imposing the test-recorded temperatures at the front face of the concrete and observing the predictions of temperature profile through the rest of the section. In general, the predictions are quite accurate. Although the model over-predicts the temperatures from ~100 °C upwards as a result of ignoring the effects of moisture evaporation, the actual rate of temperature rise (i.e. the curvature of the profiles) matches the test results very well. This suggests that the concrete properties are appropriate and also that the differential formulations are valid.

The predictions produced by the hybrid model for the temperature difference across the air gap are presented and compared with corresponding experimental data in Fig. 5. In the main, the plots demonstrate a satisfactory correlation between theoretical and experimental results. The predictions are accurate over the first 15 minutes of heating for both the 50 kW/m^2 and 35 kW/m^2 heat fluxes. The model does however tend to produce slightly un-conservative solutions for the concrete temperatures after this period, particularly when compared with the 50 kW/m^2 test results, as evident from the over-estimation of the temperature difference between the back face of the steel and the front face of the concrete (i.e. the concrete is predicted to be cooler than observed in tests and would therefore resist load for longer if structural predictions were subsequently made). This could be due to the convection within the gap and the emissivity of the two surfaces not remaining constant and this not being accounted for in the analysis, although for a typical heat transfer analysis the model performs very well.

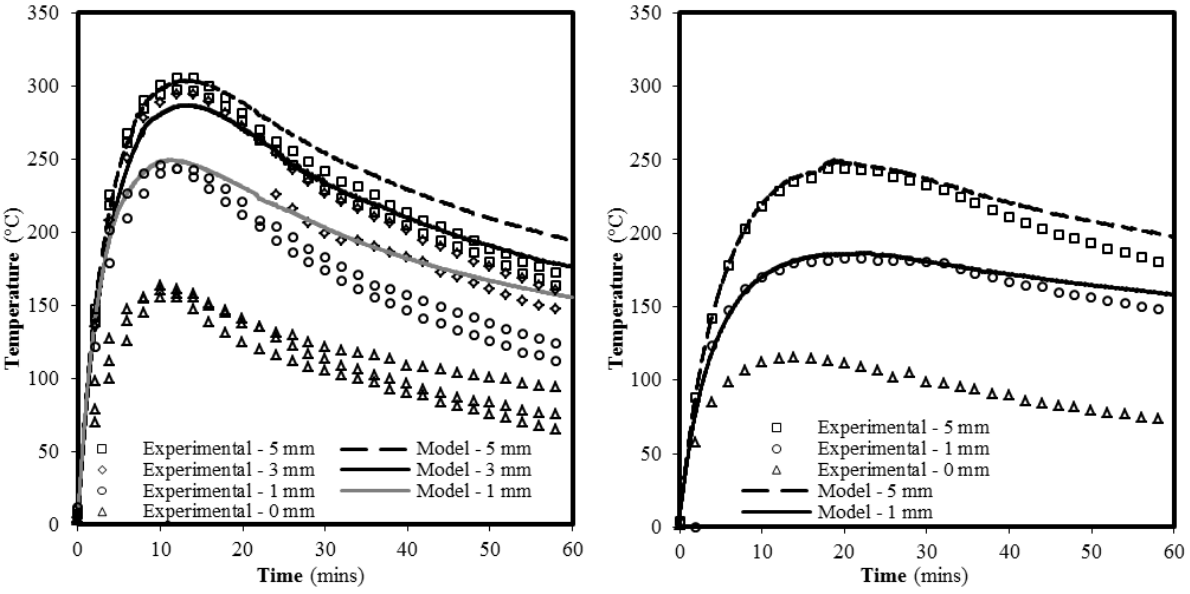

(a) (b)

Fig. 5. Comparison of predictions from hybrid model with experimental data for the temperature difference across the air gap, in specimens exposed to (a) 50 kW/m^2 heat flux; (b) 35 kW/m^2 heat flux.

Each of the solutions shown in Fig. 5 employed a specific empirical parameter, *n*, and these values are presented in Fig. 6. It is shown that as $w \rightarrow 0$, so too $n \rightarrow 0$, which is to be expected as the range of air gaps approaching 0 mm the convective effects which contribute to the conductance h_{gap} diminish and the heat transfer tends towards pure conduction. Fig. 6 indicates that *n* may also increase with increasing levels of incident heat flux, although no conclusions can be made from the results of this study as only two different heat fluxes were applied.

This study does suggest however, that an empirical function, $n(w, \dot{q}'')$, taking into account the variation of *n* with incident heat flux and air gap width, could be established for the heat transfer across an air gap between a steel plate and concrete mass. Clearly more extensive research, over greater ranges of heat flux and air gap widths, is required before a valid function for *n* can be defined. Such an empirical function could be employed to predict the 1-

D temperature profile evolution in a CFS section exposed to fire by incorporating it in the air gap conductance term, h_{gap}:

$$h_{gap} = n(w, \dot{q}'') \left(\frac{k}{L} Nu\right) \quad (24)$$

Ultimately, by incorporating a function of this type in heat transfer analyses, and indeed thermo-mechanical analyses, of CFS sections exposed to fire conditions, it may be possible to legitimately consider the development of an air gap in their structural fire design.

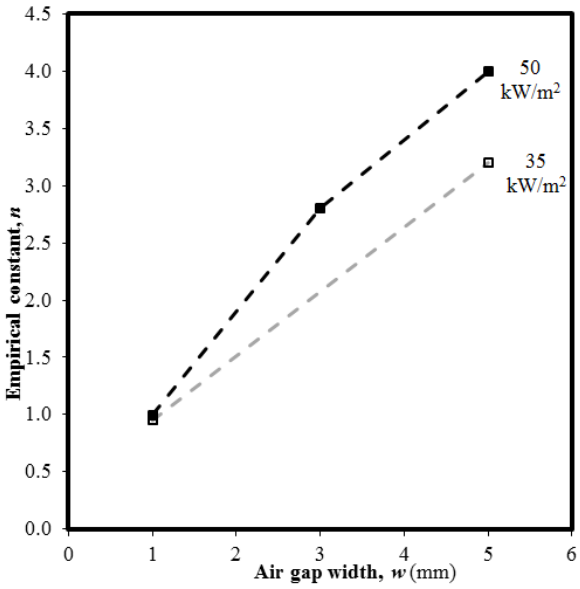

Fig.6: Variation of empirical constant, *n*, with air gap width, *w*

CONCLUSIONS AND RECOMMENDATIONS

This paper has presented a series of 15 experiments and an analytical 1-D model of an idealised infinitely large concrete filled steel hollow section (CFS). An air gap of constant width has been introduced between the steel and the concrete so that a quantified assessment of the impact of the air gap width on the heat transfer through a CFS section can be established. The significance of the air gap is of interest for the structural fire design of CFS sections. The omission of the air gap and its effects on the heat transfer within the section can lead to under-predictions of steel temperatures and over-prediction of concrete temperatures, resulting in inefficient or potentially unsafe design of CFS sections. The findings presented within this paper clearly show that:

- the formation of an air gap between steel tube and concrete core has a significant insulating influence on the heat transfer through the section; the insulating effects increase as the air gap width is increased;

- the numerical model developed was able to accurately predict the thermal response of the concrete mass as a result of an imposed temperature evolution in the steel plate; thus, a

valid 1-D heat transfer model representing the heat transfer across an air gap between steel and concrete; and

- from a comparative study of the numerical model with the results of the experimental programme, an empirical correlation parameter, *n*, was established between the heat transfer across the air gap and the width of the gap. It is anticipated that further investigation of this correlation could lead to more advanced heat transfer models of CFS columns which account for the impact of an evolving air gap at the steel-concrete boundary.

The findings of this study have highlighted that the air gap needs to be considered if accurate design of CFS sections exposed to fire are to be carried. In order to further progress from the research presented in this paper to a more practical level, it is recommended that future study focus on:

- developing a purely analytical 1-D heat transfer model so that experimentally measured steel temperature data is not required to predict the temperature profile evolution within the concrete;

- expanding the experimental programme to validate the analytical model over greater ranges of both air gap width and heat flux; in this manner, the correlation between air gap size and heat transfer across the gap could be established with greater certainty; and

- finally, research involving full-scale thermal and structural tests, in conjunction with numerical analyses that account for the formation and development of an air gap, of the complete thermo-mechanical response of loaded CFS columns.

ACKNOWLEDGEMENTS

We gratefully acknowledge the support of Arup (Fire), The Ove Arup Foundation, The Royal Academy of Engineering, and the UK Engineering and Physical Sciences Research Council. The authors also gratefully acknowledge the support of the School of Engineering at the University of Edinburgh, which is part of the Edinburgh Research Partnership in Engineering and Mathematics.

REFERENCES

Aribert JM, Renaud C, Zhao B. Simplified fire design for composite hollow-section columns. In Proceedings Of The Institution Of Civil Engineers - Structures and Buildings, 2008, 161,6, p. 325-336. doi:10.1680/stbu.2008.161.6.325.

Bejan A. Heat Transfer. John Wiley and Sons, New York, 2003.

CEN. BS EN 1994-1-2, Eurocode 4 — Design of composite steel and concrete structures — Part 1-2: Structural Fire Design. Brussels, Belgium, 2005.

CEN. NA to BS EN 1994-1-2: UK National Annex to Eurocode 4: Design of composite steel and concrete structures - Part 1-2: General rules - Structural fire design. Brussels, Belgium, 2008.

Babrauskas V. Specimen heat fluxes for bench-scale heat release rate testing. Fire and Materials, 1995, 19 (6), p. 243–252.

de Graff JGA, van der Held EFM. The relation between the heat transfer and the convection phenomena in enclosed plane air layers. Applied Scientific Research, 1952, 3(6), p. 393-409.

Ding J, Wang YC. Realistic modelling of thermal and structural behaviour of unprotected concrete filled tubular columns in fire. Journal of Constructional Steel Research, 2008, 64 (10), p. 1086–1102. doi:10.1016/j.jcsr.2007.09.014.

Incropera FP, Dewitt DP. Introduction to Heat Transfer. John Wiley and Sons, New York, 2002, p. 892.

Kodur VKR. Achieving fire resistance through steel concrete composite construction. In Proc. Structures Congress '05, 2005, New York, April 21-23, p. 1-6.

Kodur VKR. Guidelines for Fire Resistant Design of Concrete-Filled Steel HSS Columns-State-of-the-Art and Research Needs. International Journal of Steel Structures, 2007, 7 (3), p. 173–182.

Lennon T, Moore DB, Wang YC, Bailey CG. Designers' guides to the Eurocodes. London, UK: Thomas Telford Publishing, 2007.

Leon R, Griffis L. Composite Column Design. SpecWise, Modern Steel Construction, (August), 2005.

Lie TT, Kodur VKR. Fire Resistance of Steel Columns Filled with Bar-Reinforced Concrete. ASCE J. Structural Engineering, 1996, 122 (1), p.30-36.

Lie TT, Irwin RJ. Fire Resistance of Steel Columns Filled with Fibre-Reinforced Concrete. ASCE J. Structural Engineering, 1996, 122 (7), p. 776-782.

Park SH, Song K, Chung KS, Choi SM. Characteristics analysis of the performance design equations for the fire resistance of concrete-filled steel tube columns. In Proc. Fifth International Conference in Structures In Fire (SiF '08), 2008, p. 584-593. Singapore, May.

Renaud C. Improvement and extension of the simple calculation method for fire resistance of unprotected concrete filled hollow columns. CIDET Research Report 15Q, 2004, Paris, France: CIDECT.

Rush D, Bisby L, Jowsey A, Lane B. Structural fire performance of concrete-filled steel hollow sections: State of the art and knowledge gaps. In Proc. 12th International Interflam Conference, Nottingham University, July 5-7, 2010, 1, p. 57-70.

Wang YC, Orton A. Fire resistant design of concrete filled tubular steel columns. Structural Engineer 7 (October), 2008, p. 40-45.